CHAPTER IV
RESULTS AND DISCUSSION

4.1 Flow Regime

Flow pattern map was produced by varying the air and the water velocity as shown in Figure 4.1, the superficial air velocities are plotted with the superficial water velocities. This flow pattern map presents only the bubble regime, transition of bubble to slug flow regime and slug flow regime because of the limitation of equipment. The transition of bubble to slug flow can be occurred successively by increasing the superficial air velocity and keeping the superficial water velocity constant. The transition of bubble to slug flow from the experiment shows the wide range and covers all of the predicted values which were calculated by Nicklin's model and using the assumption of a void fraction of 0.1.

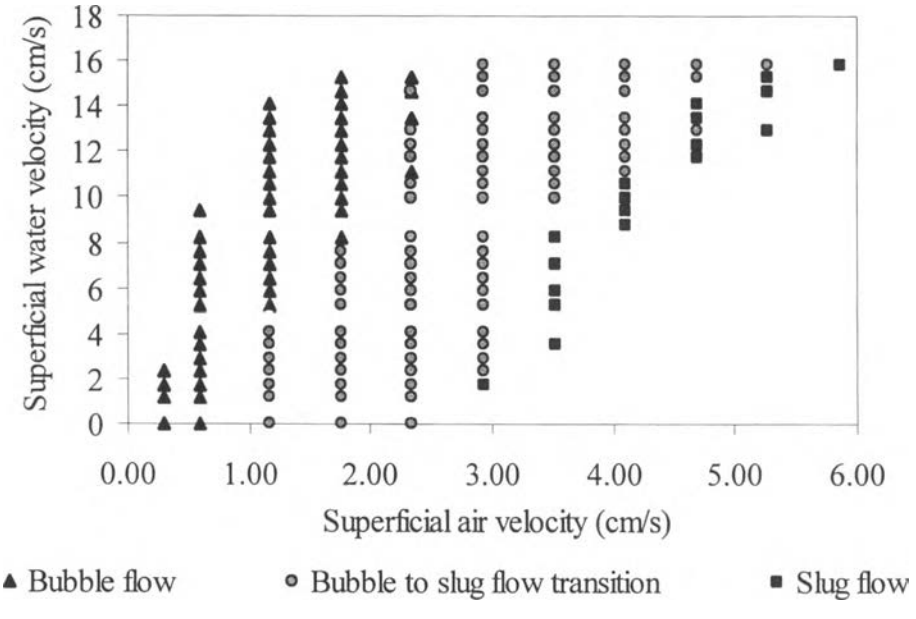

Figure 4.1 Flow pattern map produced from a column with a diameter of 1.9 cm.

4.2 Rise Velocities of Single Slug (u_b) and Slug Length

The single slugs with different lengths were generated and risen up through in the stagnant liquid. The length of single slugs was measured by recording the single slug in video camera and was studied in the range of 2.50 cm to 48.00 cm.

The independence of rise velocity of single slug with the length of slug was shown in Figure 4.2. Increasing the length of slug does not affect the rise velocity of single slug. Figure 4.3 shows the relationship between the slug length and the value of c from experiment which was calculated from equation (5). The average value of c was very close to the theoretical value which equal to 0.35.

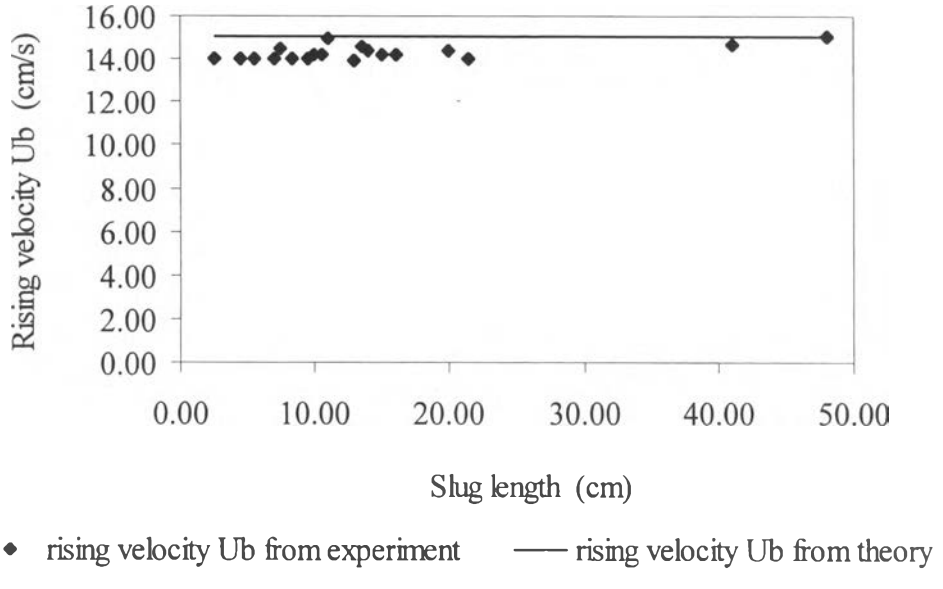

Figure 4.2 Comparison of the rising velocity from theory with the rising velocity from experiment in the column with the diameter of 1.9 cm.

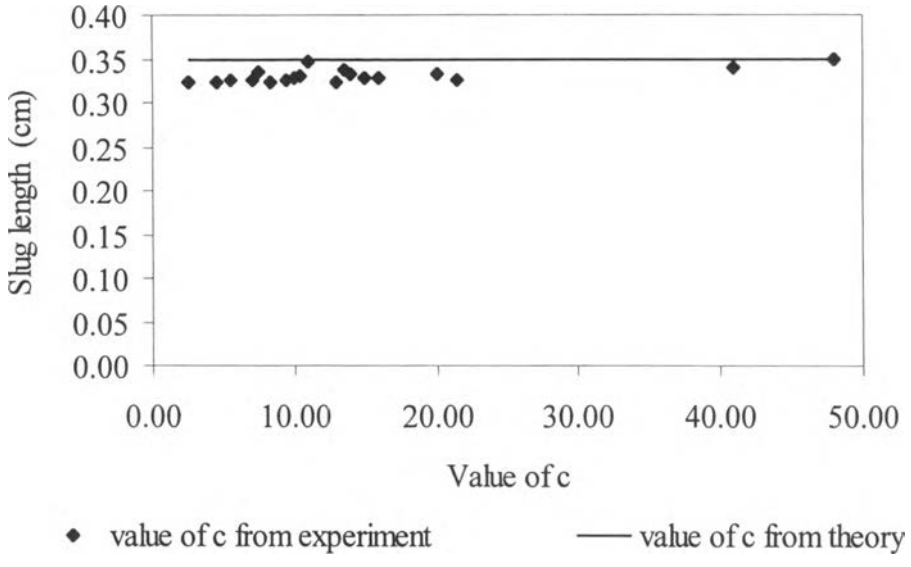

Figure 4.3 Comparison of the value of c from theory with the value of c from experiment in the column with a diameter of 1.9 cm.

4.3 Void Fractions at a Variety of Superficial Air and Superficial Water Velocities within Slug Flow

By flowing air and water upthrough the column, two valves were closed simultaneously in order to separate air and water and measure the void fraction. Figure 4.4 through Figure 4.10 show the relationship between the superficial air velocity and the void fraction. The studied range of superficial air velocity and superficial water velocity were 2.93 to 70.42 cm/s and 0 to 14.67 cm/s, respectively.

When the superficial air velocity increased whereas the superficial water velocity kept constant, the void fraction increased. The void fractions can be calculated from equation (8) and they were close to the void fractions measured from experiments. There were some deviations at the higher superficial air velocity, in which they probably occurred the transition of slug to churn flow. However, this equation can predict the satisfactory void fraction and an error from experimental results does not exceed 7 %.

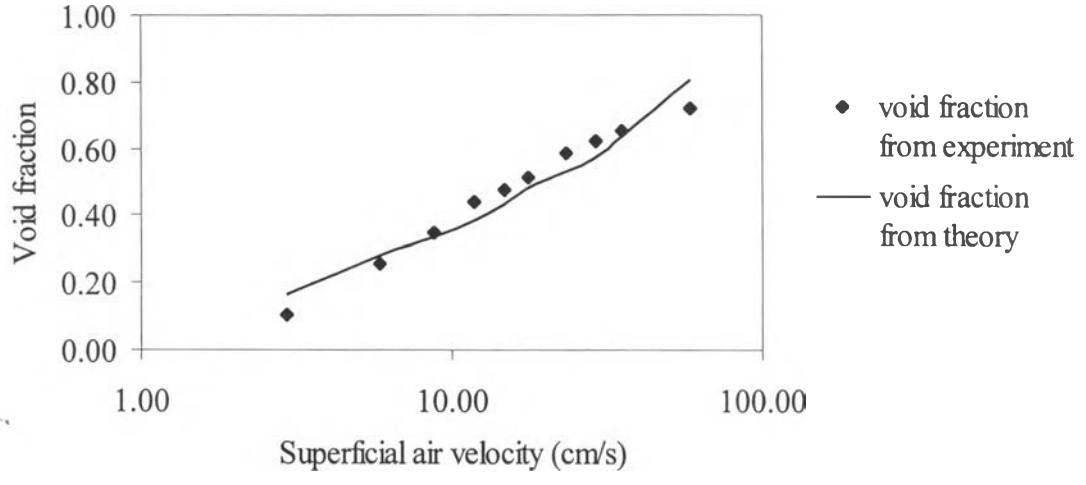

Figure 4.4 Comparison of the void fraction from theory with the void fraction from experiment at 0 ml/min water flow rate.

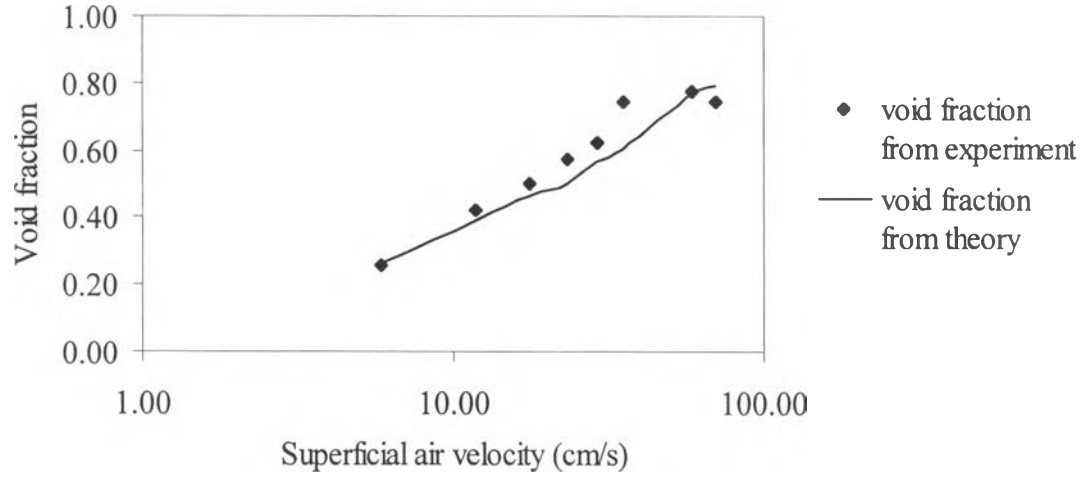

Figure 4.5 Comparison of the void fraction from theory with the void fraction from experiment at 200 ml/min water flow rate.

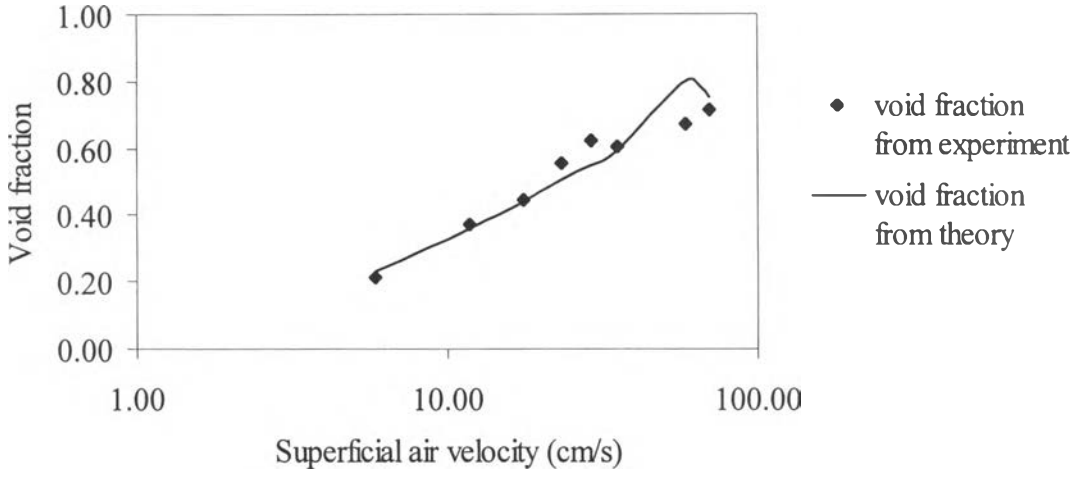

Figure 4.6 Comparison of the void fraction from theory with the void fraction from experiment at 500 ml/min water flow rate.

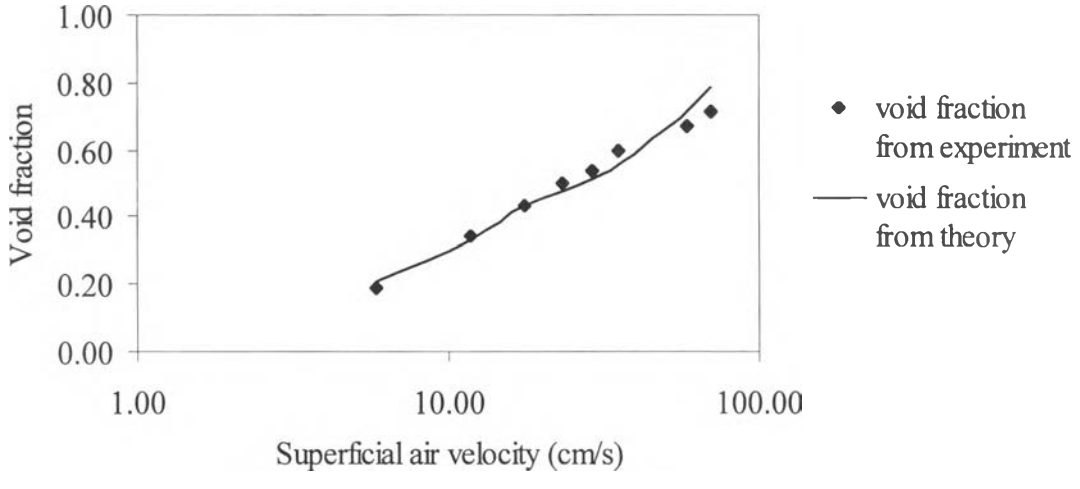

Figure 4.7 Comparison of the void fraction from theory with the void fraction from experiment at 1000 ml/min water flow rate.

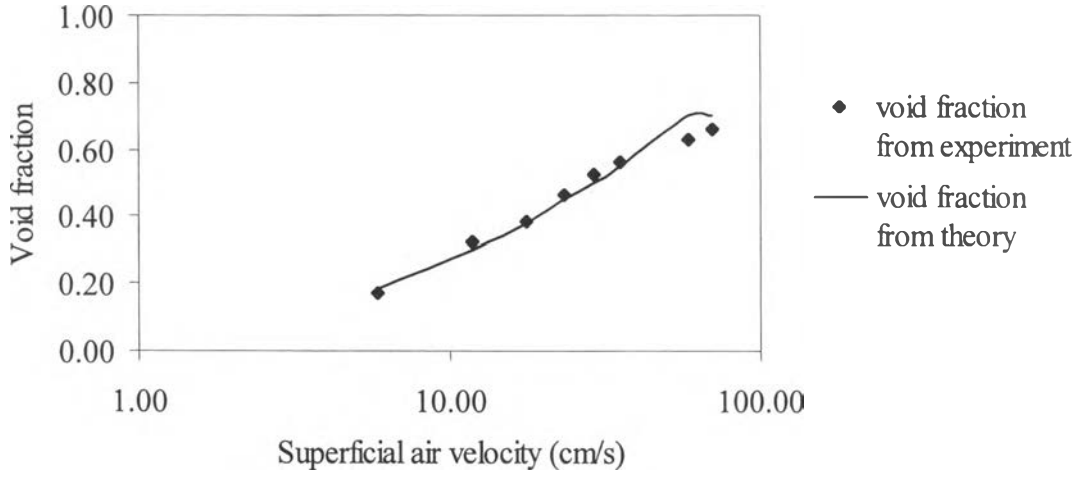

Figure 4.8 Comparison of the void fraction from theory with the void fraction from experiment at 1500 ml/min water flow rate.

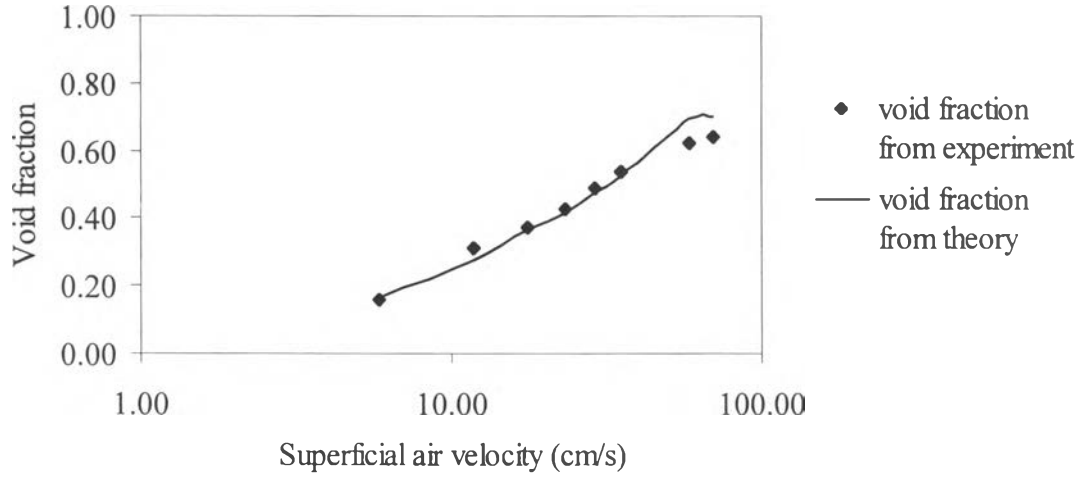

Figure 4.9 Comparison of the void fraction from theory with the void fraction from experiment at 2000 ml/min water flow rate.

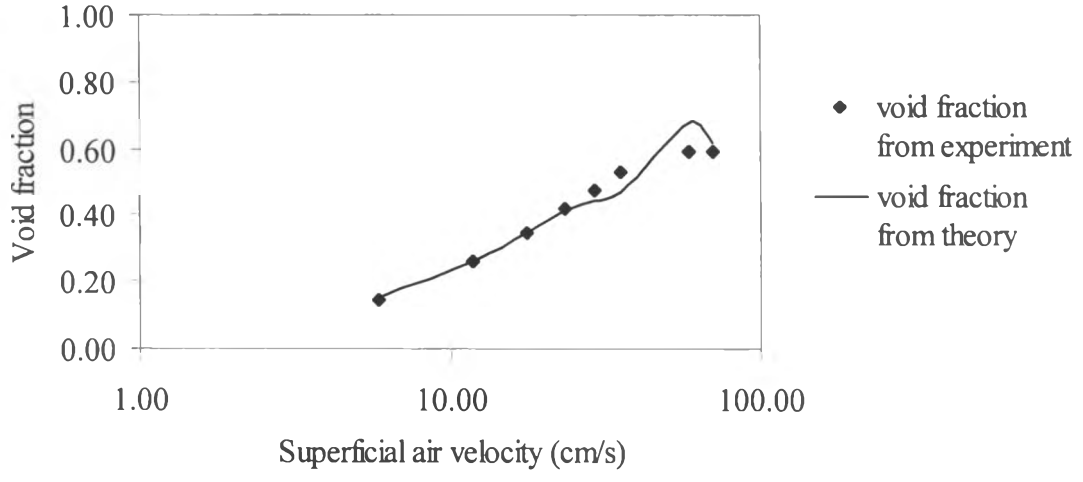

Figure 4.10 Comparison of the void fraction from theory with the void fraction from experiment at 2500 ml/min water flow rate.

4.4 Rise Velocities of Continuously Generated Slug (u_s)

The continuously generated slug were generated with different superficial air and water velocities in the same range as used in the determination of the void fractions. The results are shown in Figure 4.11 through Figure 4.17 in which the rise velocity of continuously generated slug is plotted with the superficial air velocity. While the superficial air velocity increased, the rise velocity increased linearly. The theoretical rise velocities can be calculated by equation (6) and they agree well with the rise velocities from experiments with an error of less than 5 %.

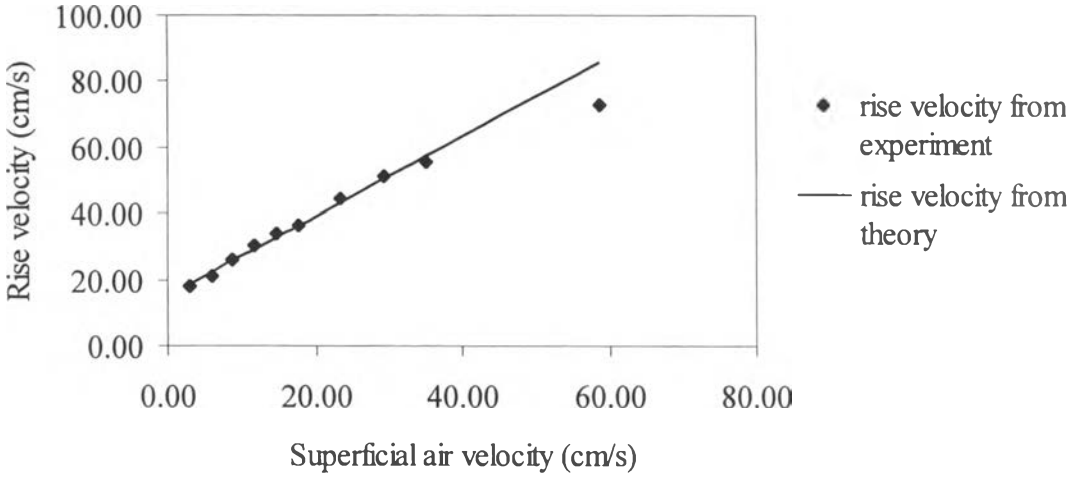

Figure 4.11 Comparison of rise velocity of continuously generated slugs between theory and experiment at 0 ml/min water flow rate.

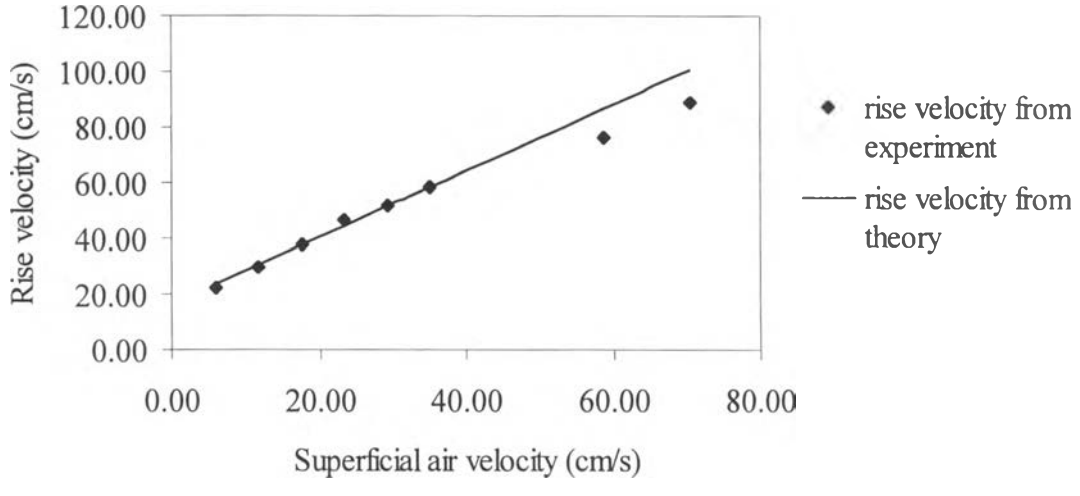

Figure 4.12 Comparison of rise velocity of continuously generated slugs between theory and experiment at 200 ml/min water flow rate.

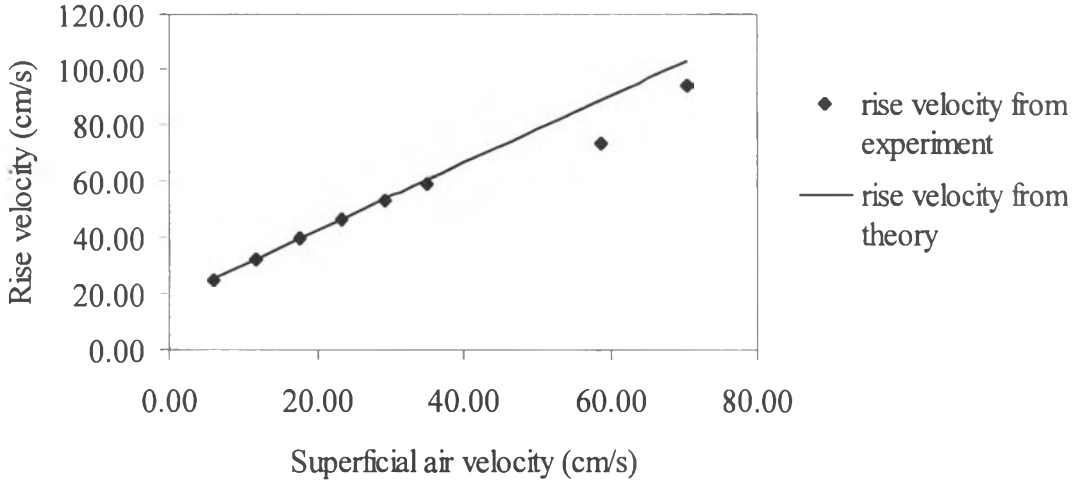

Figure 4.13 Comparison of rise velocity of continuously generated slugs between theory and experiment at 500 ml/min water flow rate.

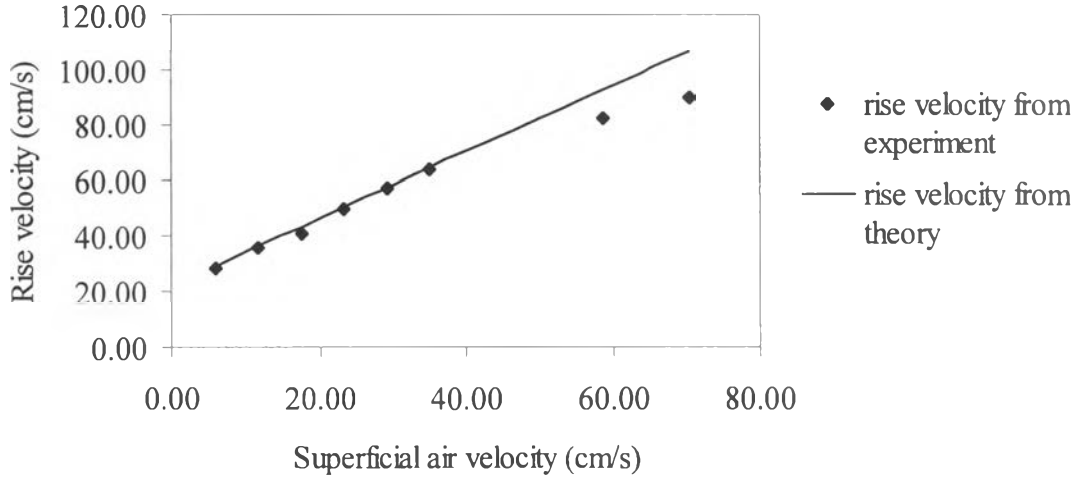

Figure 4.14 Comparison of rise velocity of continuously generated slugs between theory and experiment at 1000 ml/min water flow rate.

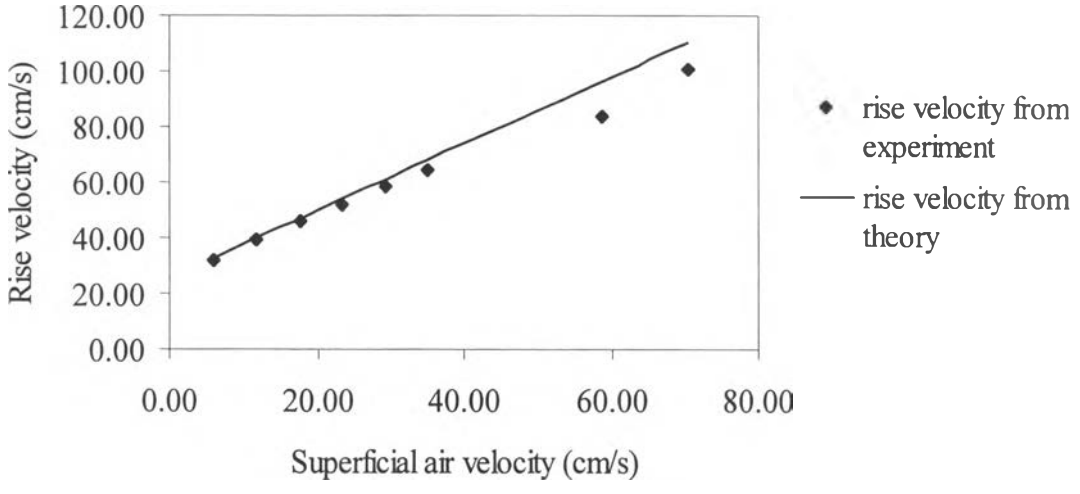

Figure 4.15 Comparison of rise velocity of continuously generated slugs between theory and experiment at 1500 ml/min water flow rate.

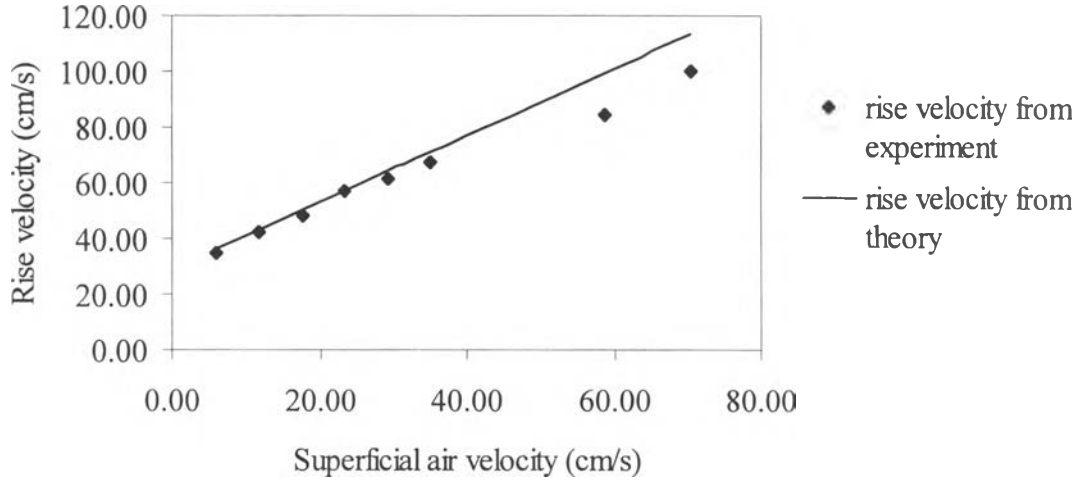

Figure 4.16 Comparison of rise velocity of continuously generated slugs between theory and experiment at 2000 ml/min water flow rate.

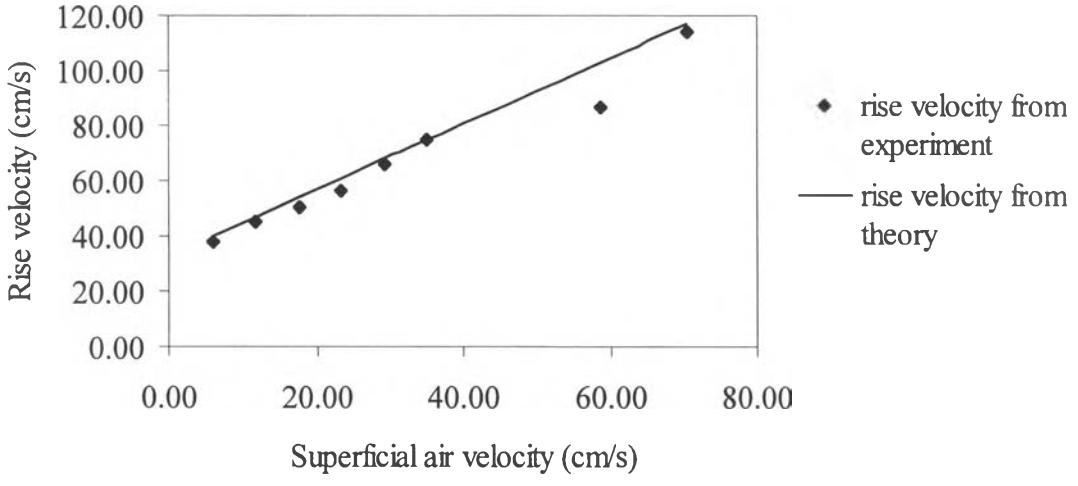

Figure 4.17 Comparison of rise velocity of continuously generated slugs between theory and experiment at 2500 ml/min water flow rate.

4.5 Air-Lift Pump Operation

Figure 4.18 shows the relationship between the initial height of water in main and reservoir columns and the superficial air velocities for incipient air-lift pump operation. Increasing the initial height of water in main and reservoir columns caused air velocity for incipient air-lift pump to decrease. At no higher initial height of water in main and reservoir column, the required air velocity from experiment agreed well with the predicted required air velocity. The absolute average error of this experiment is less than 13.05%

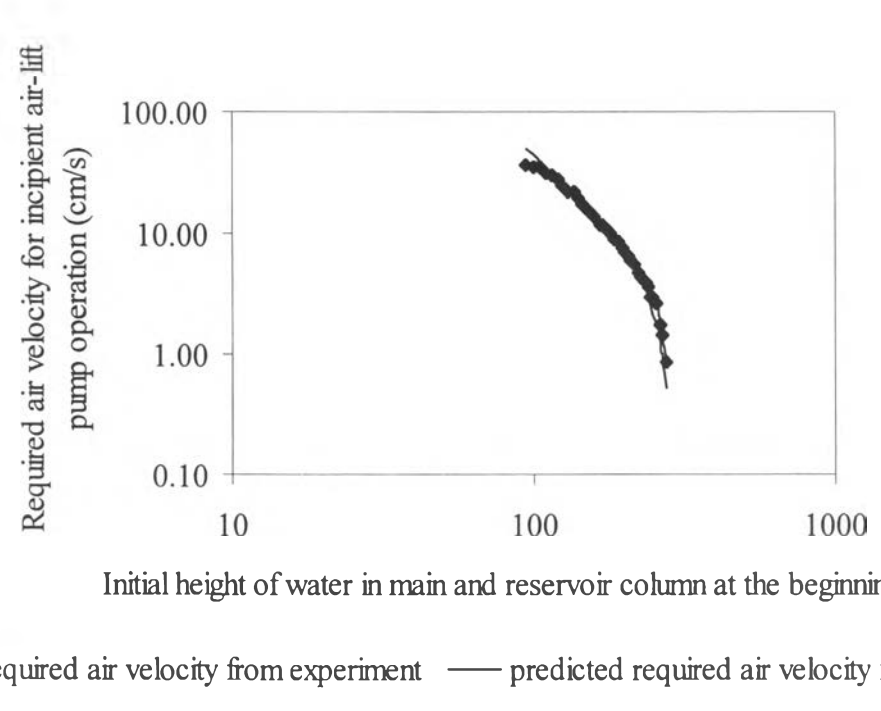

Figure 4.18 Comparison of required air velocity for incipient air-lift pump operation from theory with those from experiments at different initial heights of water in main column and reservoir column.

4.6 Slug Flow Analysis

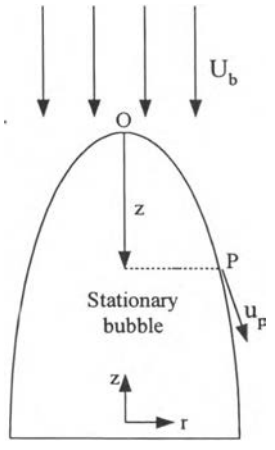

Figure 4.19 The stationary bubble in moving downward liquid.

The rise velocity of bubble (u_b) can be determined from potential-flow theory by considering an observer travelling upwards with a gas slug. The gas is apparently stationary, with liquid streaming downwards past it in potential flow, in which viscosity is insignificant. The liquid velocities can be deduced by a finite-element computer solution of Laplace's equation (Wilkes and La Valle, 1990) as shown in equation 11

$$\frac{\partial^2 \phi}{\partial r^2} - \frac{1}{r}\frac{\partial \phi}{\partial r} + \frac{\partial^2 \phi}{\partial z^2} = 0 \qquad (11)$$

where ϕ is the potential function and the radial velocity and axial velocity components of liquid around the gas slug are given by

$$u_r = -\frac{\partial \phi}{\partial r} \qquad (12)$$

$$u_a = -\frac{\partial \phi}{\partial z} \qquad (13)$$

The shape of the slug was adjusted by comparing the liquid velocity at the free surface of the slug from potential flow theory with liquid velocity at all heights below the nose of the slug from Bernoulli's equation which is shown in equation (14)

$$u_p = \sqrt{2gh} \qquad (14)$$

where h is the vertical distance between O and P.

The results of the liquid velocity from potential-flow theory and Bernoulli's equation at the free surface of slug are shown in Table 4.1. Table 4.2 shows rise velocity of bubble and constant value from FEM Program (Thipkunthod, 2002) which gave a good agreement with the theoretical values within the relative error less than 1%.

Table 4.1 Liquid velocity at the free surface from potential-flow theory and Bernoulli's equation.

z (cm)	V from potential-flow theory (cm/s)	V from Bernoulli (cm/s)	% Error
0.00	0.00	0.00	0.00
0.02	6.23	6.29	0.06
0.05	10.00	9.91	0.10
0.09	13.32	13.29	0.13
0.15	17.23	17.16	0.17
0.23	21.27	21.24	0.21
0.34	25.77	25.83	0.26
0.48	30.72	30.69	0.31
0.66	35.96	35.99	0.36
0.90	42.14	42.02	0.42
1.20	48.66	48.52	0.49

Table 4.2 Comparison of rise velocity of bubble and c from FEM Program with those from theory.

	FEM Program	Theory	% Error
Rise velocity, u_b	15.096	15.100	0.026
Constant, C	0.349	0.350	0.286

Figure 4.20 presents the shape of single slug from FEM Program compare to the shape of single slug from experiment. The result shows that shape of single slug from FEM Program was quite closed to the real shape.

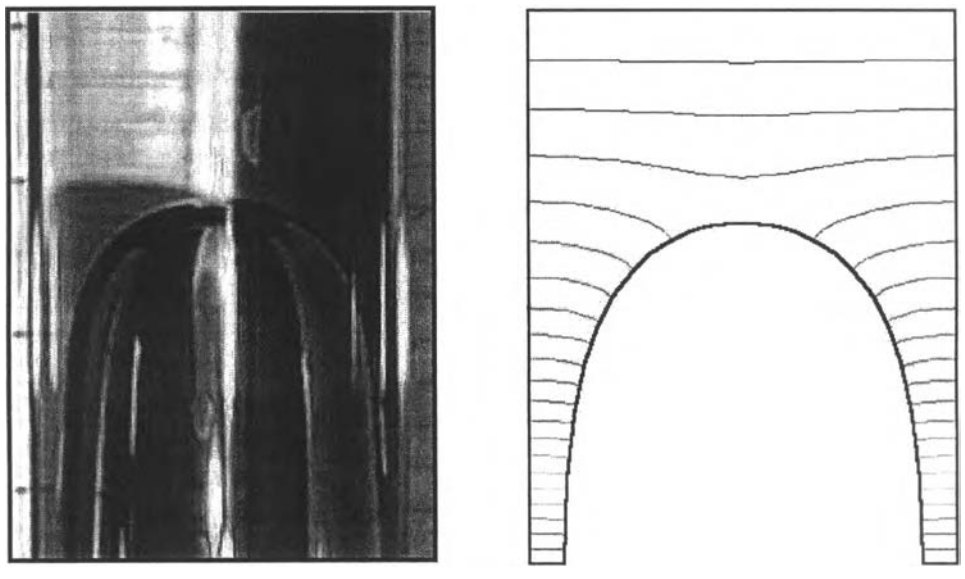

(a) actual slug (b) slug from FEM analysis

Figure 4.20 Comparison of the shape of single slug from FEM Program with one from experiment in a column with a diameter of 1.9 cm.

4.7 Flooding Line

The flooding was studied at a variety of water mass velocities and air mass velocities in the range of 0.15 to 0.60 g/cm^2.s and 0 to 11.66 g/cm^2.s, respectively. Plastic raschig rings and ceramic balls were selected as packing elements for determining the difference of shape and size. Moreover, two different heights of packing (60 and 80 cm) were also investigated. The visual inspection and the graphical detection were used in order to find the air mass velocity that causes the flooding at each water mass velocity.

Table 4.3 Gas mass velocities at flooding in difference types and heights of packing

Water mass velocity (g/cm^2.s)	Air mass velocity at flooding (g/cm^2.s)			
	60 cm of packing height		80 cm of packing height	
	Ceramic ball	Plastic raschig ring	Ceramic ball	Plastic raschig ring
0.15	8.56	6.61	6.22	7.00
0.24	5.83	6.61	5.83	5.83
0.30	4.67	5.83	5.44	5.44
0.36	5.44	5.44	5.06	3.89
0.45	2.72	4.28	4.28	3.50
0.60	2.33	2.53	2.14	1.94

Then the results are plotted in the Eckert type chart which are very well-known as Generalized Pressure Drop Correlation (GDPC). The GDPC is an empirical correlation between the generalized superficial gas velocity head and the ratio of the superficial velocity heads of liquid and gas. The ordinate and abscissa of the GDPC are conceptually attractive because they imply that interaction of gas and liquid influences pressure drop and flooding. The Eckert type charts in Figure 4.21 and 4.22 show that ceramic balls gave higher region of normal operation or lower region of flooding than did plastic raschig rings at both of two heights of packing. But at different heights of the same packing, the Eckert type charts gave the same transition trend between normal and flooding operation which are shown in Figure 4.23 and 4.24

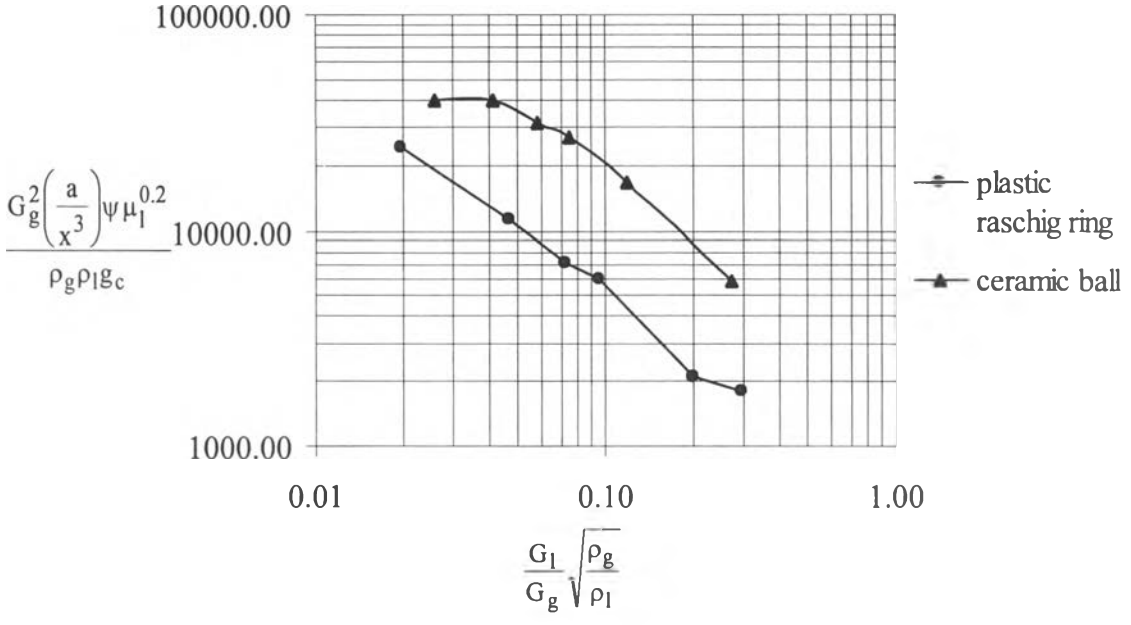

Figure 4.21 Eckert type chart of plastic raschig rings and ceramic balls at the height of packing 60 cm.

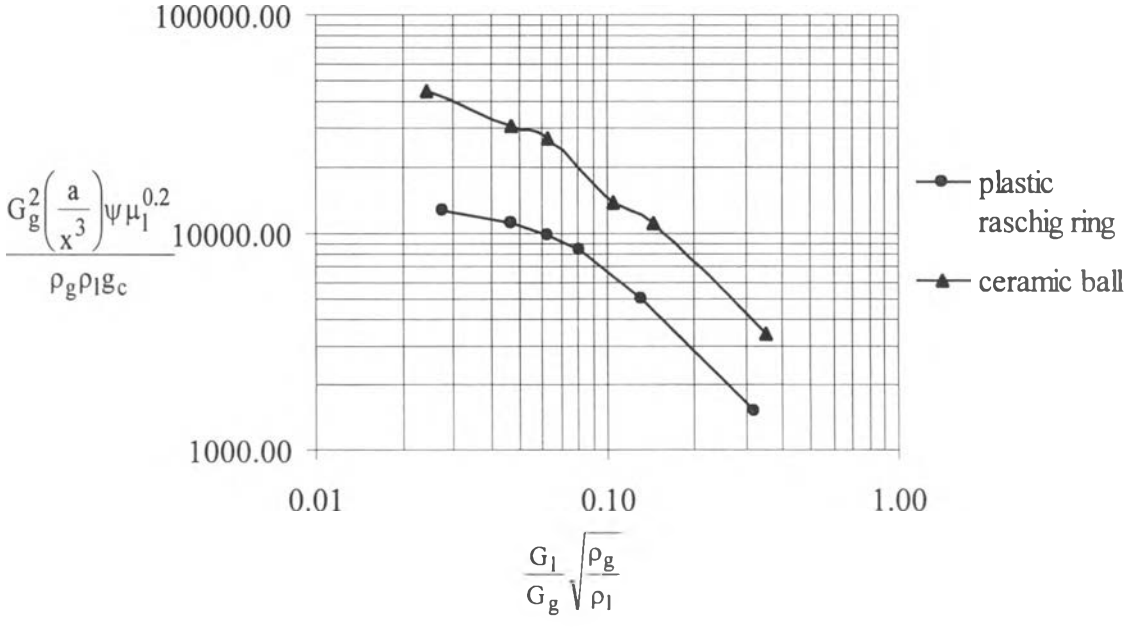

Figure 4.22 Eckert type chart of plastic raschig rings and ceramic balls at the height of packing 80 cm.

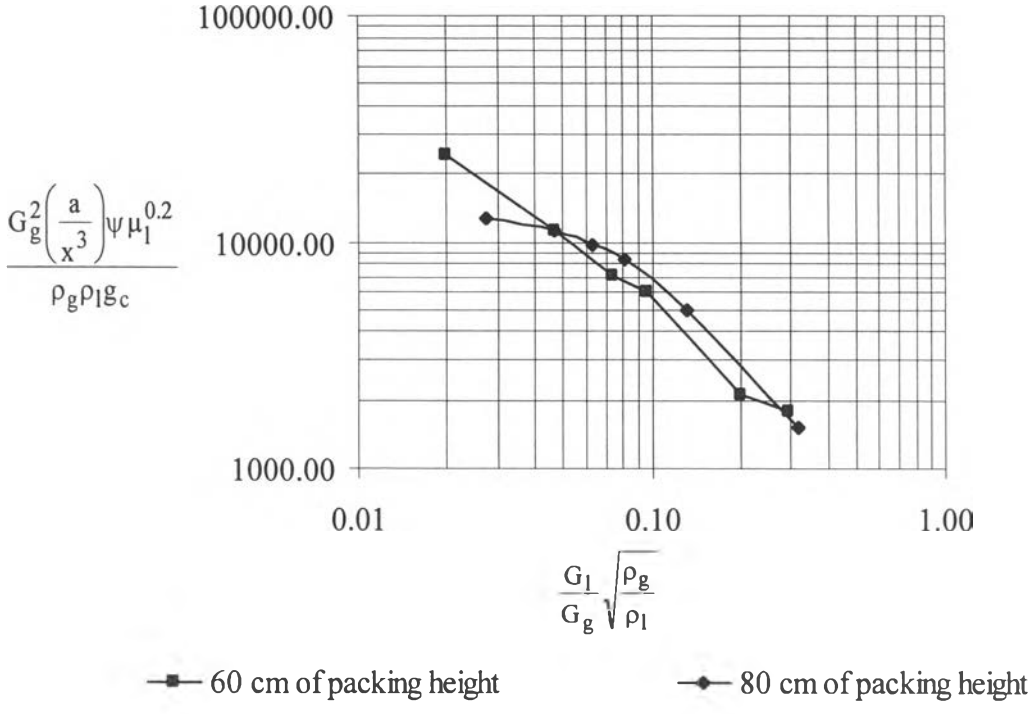

Figure 4.23 Eckert type chart of plastic raschig rings at different heights of packing.

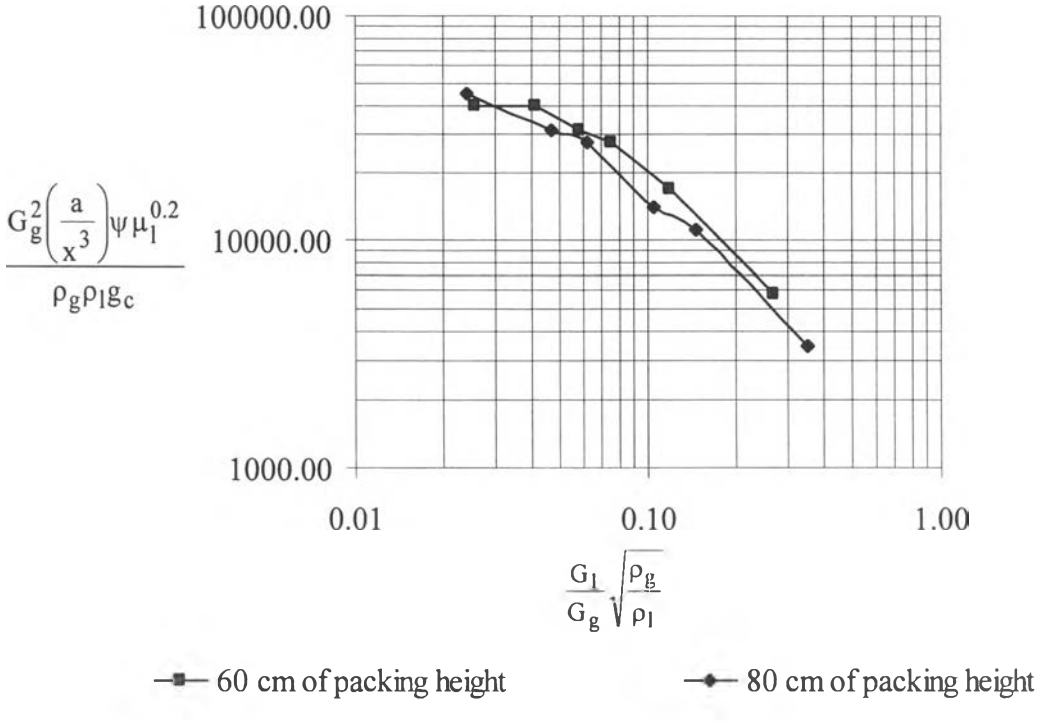

Figure 4.24 Eckert type chart of ceramic balls at different heights of packing.

4.8 Pressure Drop with Air Mass Velocities and Water Mass Velocities

The experiment was carried out with ceramic balls and plastic raschig rings at the different heights of packing of 30, 60, and 80 cm, respectively.

The logarithmic plot of pressure drop and gas mass velocity also shows the phenomenon that occurs at difference water mass velocities which are 0.15, 0.30 and 0.45 g/cm^2.s, as illustrated in Figure 4.25 through 4.30. When the gas mass velocity remained constant, the pressure drop increased with an increase in the water mass velocity. This occurred because as the water filled the voids in the column, the cross-sectional area available for air flow was reduced. Furthermore, at higher air mass velocity, the rate of change of pressure drop increased more rapidly. This is owing to liquid holdup increased with increasing gas flowrate, and this gas flowrate was called the loading point. Above this gasflowrate, a greater amount of liquid holdup in the column was observed and it reached the flooding point. At this point, water was built up on the top of the packing and sprayed out of the column. Most of the experiments show the same results in both different types and heights of packing.

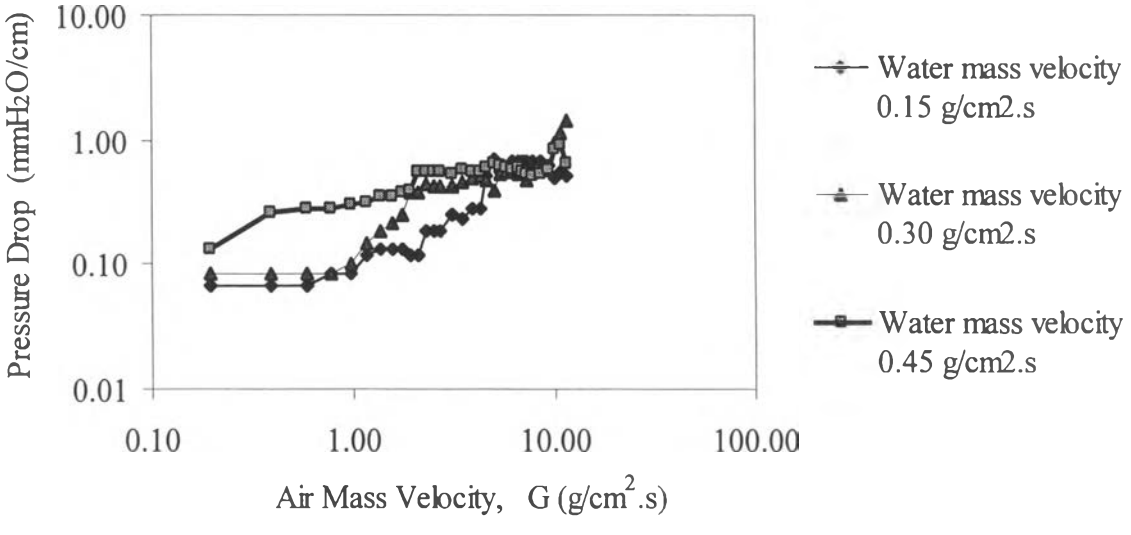

Figure 4.25 Determination of pressure drop and air mass velocities at different water mass velocities with the height of 30 cm plastic raschig rings.

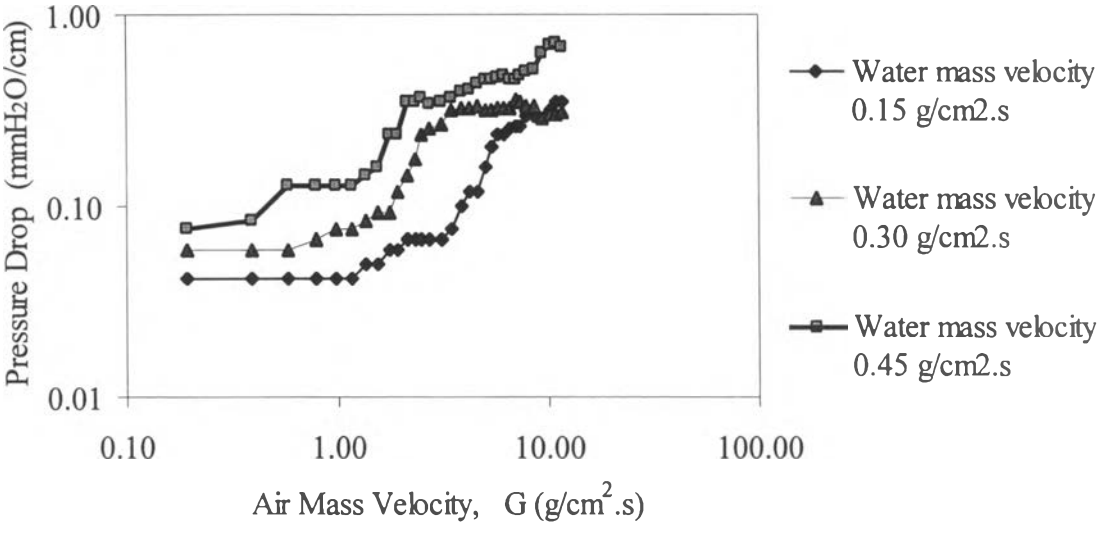

Figure 4.26 Determination of pressure drop and air mass velocities at different water mass velocities with the height of 60 cm plastic raschig rings.

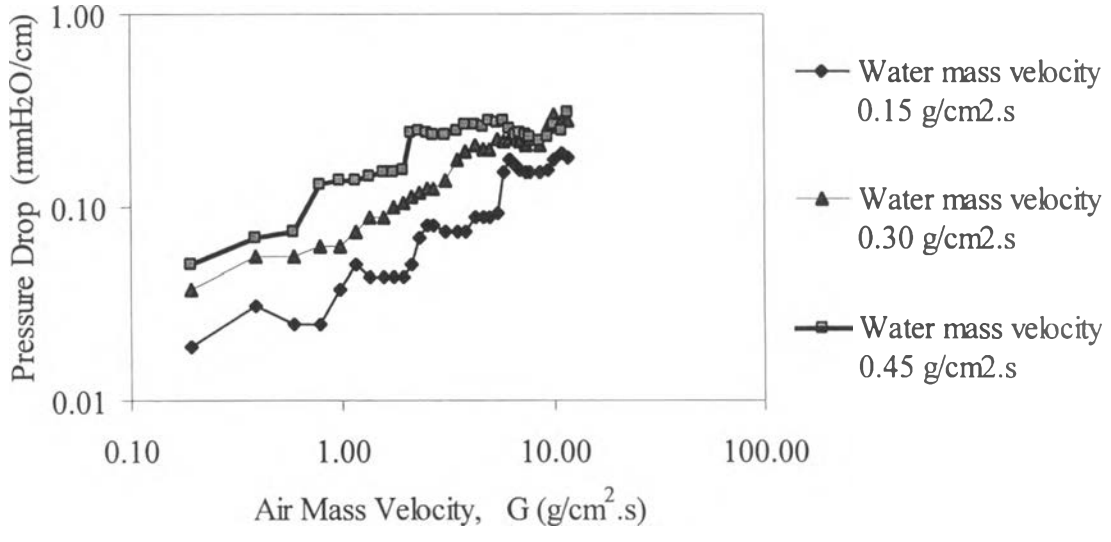

Figure 4.27 Determination of pressure drop and air mass velocities at different water mass velocities with the height of 80 cm plastic raschig rings.

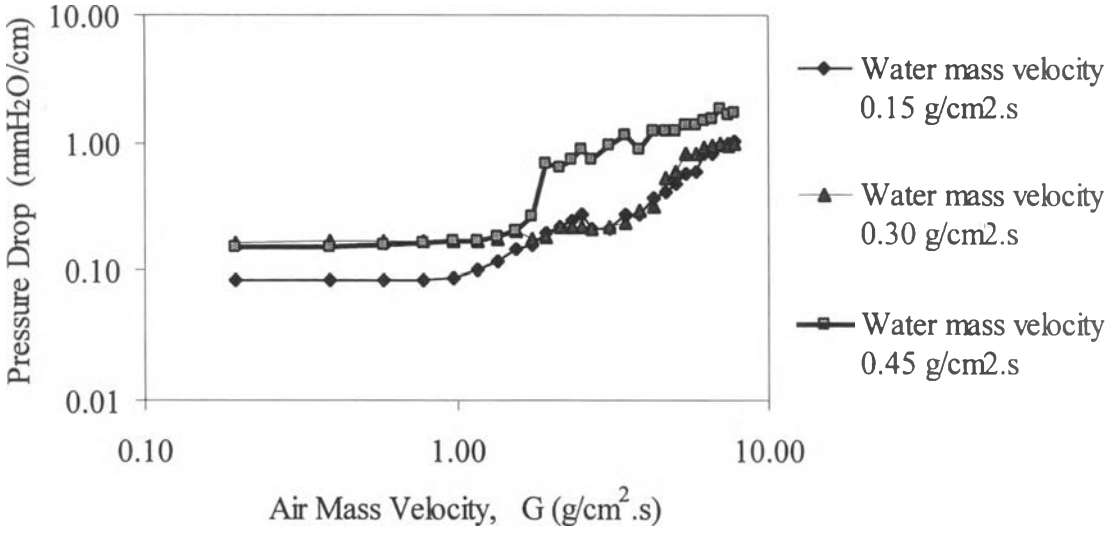

Figure 4.28 Determination of pressure drop and air mass velocities at different water mass velocities with the height of 30 cm ceramic balls.

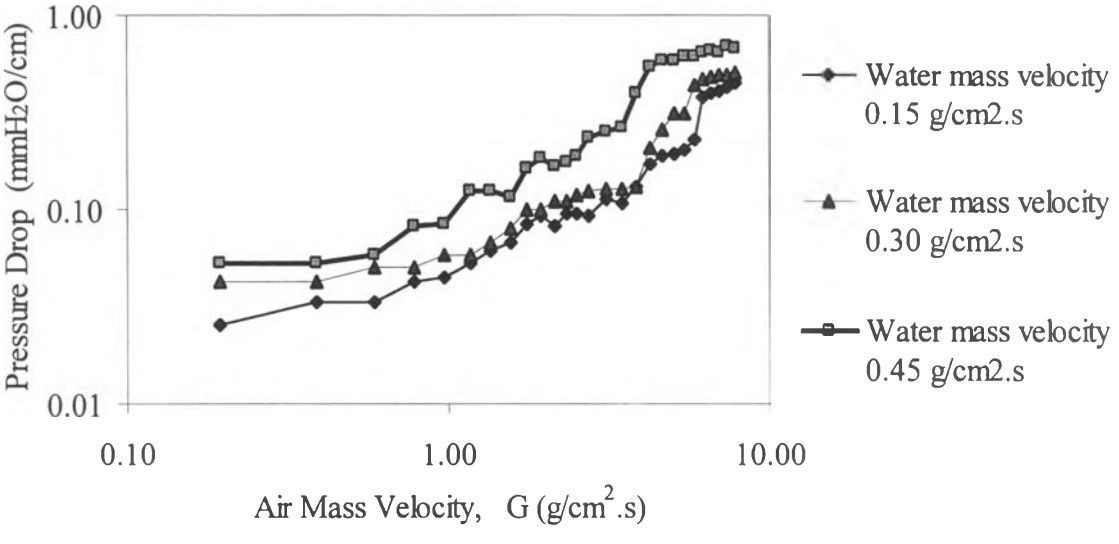

Figure 4.29 Determination of pressure drop and air mass velocities at different water mass velocities with the height of 60 cm ceramic balls.

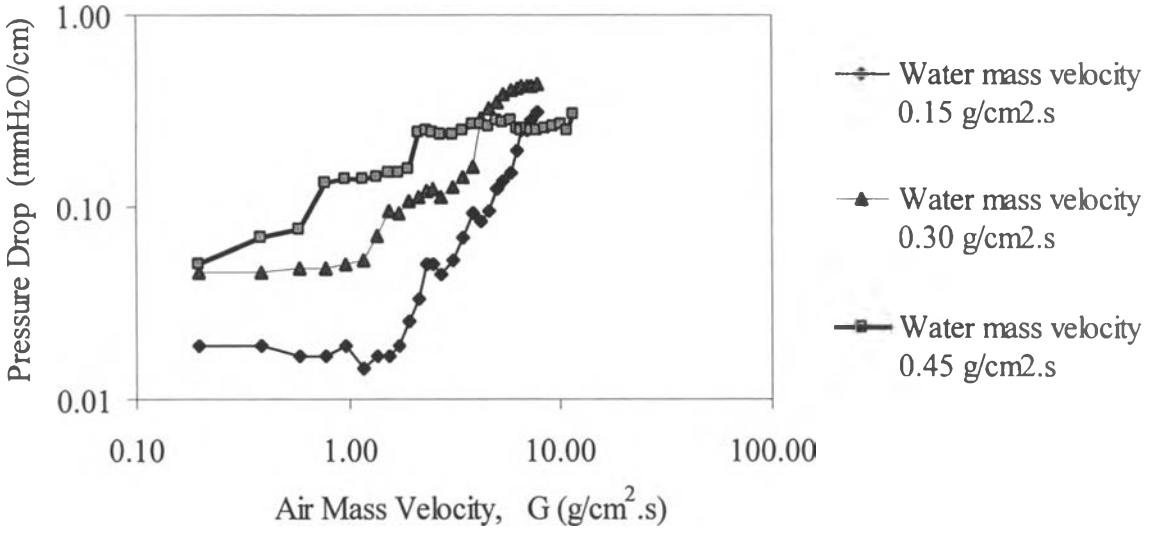

Figure 4.30 Determination of pressure drop and air mass velocities at different water mass velocities with the height of 80 cm ceramic balls.